IRON OXIDE NANOPARTICLES AS A CONTRAST AGENT FOR THERMOACOUSTIC TOMOGRAPHY

A Thesis

by

AARON LOPEZ KEHO

Submitted to the Office of Graduate Studies of
Texas A&M University
in partial fulfillment of the requirements for the degree of

MASTER OF SCIENCE

August 2006

Major Subject: Biomedical Engineering

IRON OXIDE NANOPARTICLES AS A CONTRAST AGENT

FOR THERMOACOUSTIC TOMOGRAPHY

A Thesis

by

AARON LOPEZ KEHO

Submitted to the Office of Graduate Studies of
Texas A&M University
in partial fulfillment of the requirements for the degree of

MASTER OF SCIENCE

Approved by:

Chair of Committee,	Kenith Meissner
Committee Members,	Lihong Wang
	Jaime Grunlan
Head of Department,	Gerard Coté

August 2006

Major Subject: Biomedical Engineering

ABSTRACT

Iron Oxide Nanoparticles as a Contrast Agent for
Thermoacoustic Tomography. (August 2006)
Aaron Lopez Keho, B.S., Rice University
Chair of Advisory Committee: Dr. Kenith Meissner

An exogenous contrast agent has been developed to enhance the contrast achievable in Thermoacoustic Tomography (TAT). TAT utilizes the penetration depth of microwave energy while producing high resolution images through acoustic waves. A sample irradiated by a microwave source expands due to thermoelastic expansion. The acoustic wave created by this expansion is recorded by an ultrasonic transducer. The water content in biological samples poses an obstacle, as it is the primary absorber of microwave radiation. The addition of an exogenous contrast agent improves image quality by more effectively converting microwave energy to heat. The use of iron oxide nanoparticles in MRI applications has been explored but super paramagnetic iron oxide nanoparticles (SPION) have benefits in microwave applications, as well. Through ferromagnetic resonance, SPION samples more effectively convert microwave energy into heat. This transduction to heat creates significantly larger thermoacoustic waves than water, alone. Characterization of the SPION samples is executed through TAT, TEM, XPS, EDS, and a vector network analyzer with a dielectric probe kit. One-dimensional and phantom model imaging with an iron oxide nanoparticle contrast agent provide a two-fold improvement in contrast at current system configurations. Further enhancement is possible through adjustments to the nanoparticles and TAT system.

To my mother, father, and brother

TABLE OF CONTENTS

Page

LIST OF FIGURES

I. INTRODUCTION

The importance of early detection is obvious in the diagnosis of cancer. Still, many common imaging technologies used today may only identify lesions after the cancer has undergone the majority of its natural history. By this point, the cancer is potentially lethal.

Current imaging methods, such as magnetic resonance imaging and ultrasound, are mature technologies and have reached limitations in detecting tumors smaller than 1 cm in diameter [1]. However, the combination of existing techniques allows early identification of these lesions and increases the success of treatment. New promising methods, such as thermoacoustic tomography (TAT), have been developed which allow the identification of possibly harmful tumors in their early stages [2-6].

Thermoacoustic tomography takes advantage of the depth penetration of microwave energy and the resolution of acoustic waves. In TAT, A biological sample is irradiated with microwave energy causing thermoelastic expansion. From here, an ultrasonic transducer records the thermoacoustic wave created by the deformation of the sample. Although this system has provided a significant improvement in medical imaging, there are still obstacles to overcome. Water in biological samples is the primary absorber of microwave energy. This presence of water enables TAT images to be acquired but also creates contrast because the absorption by water is much stronger than the remainder of the sample. To improve the contrast of a biological sample, an exogenous contrast agent may be added. Recently there has been work suggesting super paramagnetic iron oxide nanoparticles (SPION) have microwave properties that will serve as a contrast agent [7]. Through ferromagnetic resonance [8,9], super paramagnetic nanoparticles couple to the microwave irradiation and absorb energy. In doing so, additional heat is created,

---

This thesis follows the style of *Nanotechnology*.

increasing the amplitude of the thermoacoustic waves. The goal of this research is to develop an exogenous contrast agent that will enable more effective imaging acquisition in the thermoacoustic tomography system.

II. CONTRAST IN THERMOACOUSTIC TOMOGRAPHY

2.1 Medical Imaging: Penetration Depth, Resolution, and Contrast

Ideal medical imaging modalities provide excellent penetration depth, resolution (spatial/temporal), and contrast. Yet, current imaging modalities generally excel in only one or two of these areas.

For example, optical coherence tomography [10,11] provides good contrast and submicron spatial resolution. This interferometric, non-invasive imaging modality utilizes a broadband light source that is split into two paths. One path irradiates the sample, while a reference path is commonly incident upon a mirror. Light from both paths returns to a detector that records interference patterns. By adjusting the path length of the reference arm, the phase of the reference beam with respect to the scattered light from the specimen changes. This change causes variation in the interference pattern. Yet, as in all optical techniques, the penetration depth is generally limited to one millimeter.

Optical microscopy enjoyed a significant advancement with the development of confocal microscopy [12-14]. By adding a small, pinhole aperture to the observation, a large majority of unfocused scattered light is eliminated. In a simplified set up, a sample is placed in the laser beam path, focused with a lens. The small aperture allows control over the depth plane in which the observer wishes to see. Any light that is not at the focal plane of the lens will be removed by the pinhole. The result is clearer images that do not suffer from blurring due to unfocused light. Generally, confocal microscopy provides horizontal resolution of 0.2 micrometers and vertical resolution of 0.5 micrometers.

To improve contrast in optical imaging, contrast agents, such as indocyanine green, are added to a sample. In single photon microscopy, a fluorophore absorbs one photon. The energy of the single photon is sufficient enough to excite the fluorophore. As the

fluorophore returns to its relaxed state, energy is released in the form of light. The contrast agents function as labels within the sample.

For multiphoton microscopy, a single photon does not have enough energy to excite the fluorophore [15]. Instead, two or more photons are required to provide sufficient energy to raise the fluorophore to an excited state. The probability of this occurring is very low so a high flux of photons is necessary. The highest likelihood of two photons incident upon the same fluorophore is at the focal point of the imaging system. As a result, the user can highly specify the region of interest as only fluorophores at the focal point are likely to excite and emit light. Additionally, the reduced energy of the photons is less likely to adversely affect biological samples. Still, penetration depth is limited to millimeters.

Apart from optical imaging techniques, magnetic resonance imaging is another non-ionizing imaging modality. Unlike optical techniques, MRI yields excellent penetration depth but suffers from contrast challenges. Despite the complex nature of this technology, MRI has become a staple of biomedical imaging [16-18]. Hydrogen nuclei in biological samples align either parallel or anti-parallel to a static magnetic field. As the magnetic dipole moments of the nuclei precess about this field, an orthogonal radio frequency pulse excites the nuclei into a non-aligned, elevated state. The relaxation time for these magnetic moments is recorded and processed for imaging. In MRI, there are two main relaxation times, T1 and T2. The first relaxation time is longitudinal and generally around one second. The transverse relaxation time usually is on the order of hundreds of milliseconds.

To specify the imaging field, a second magnetic field gradient is applied. By adjusting this field, images can be taken along planes and reconstructed into three-dimensional images. Additionally, contrast agents haven been developed [19-25] to improve contrast challenges in MRI.

MRI benefits from high resolution, near 1mm, and its non-invasive design. However, the equipment for this technique is large and very expensive. In addition, extra care must be taken with patients. Any metal in or on the patient may be very dangerous due to the large magnetic fields needed to create the field gradients. This imaging modality has found use in a wide range of applications. From measuring brain activity to identifying cancerous lesions, MRI is an invaluable tool for biomedical imaging.

On the opposite end of medical imaging system cost, ultrasonography provides excellent penetration depth and spatial resolution [26-29]. Obstetric sonography is the most well known form of ultrasonography. Here, short pulses from an array of piezoelectric transducers create an ultrasonic wave. The same transducers record the echoes received from the sample under test.

The ultrasonic frequency can be changed to adjust penetration depth. This, however, comes at the cost of resolution. As penetration depth increases, the longer wavelengths provide less precise resolution information. The largest drawback to ultrasonography is contrast. The effect of various tissues within the body on the acoustic wave does not vary enough to provide sufficient contrast in images.

Ultrasonography enables real-time imaging, in addition to good penetration depth, which is impossible with optical imaging. Ultrasonography is relatively inexpensive [30], non-ionizing, and non-invasive.

These imaging modalities have played important roles in research and medical practice. However, to most effectively analyze biological samples, images must have sufficient contrast, penetration depth, and resolution. While no single imaging modality described here satisfies this criterion, a combination of existing techniques can provide the desired imaging capabilities.

2.2 Thermoacoustic Tomography

From analyzing current imaging modalities, one of the primary drawbacks of optical imaging techniques is penetration depth. Short wavelength light quickly scatters upon entering biological samples. To improve penetration depth, excitation sources with longer wavelengths must be used. However, the increase in wavelength reduces the resolution of the images. In order to acquire high resolution images with good penetration depth, hybrid imaging modalities have been developed.

Thermoacoustic tomography (TAT) utilizes microwave energy as the excitation source. Microwaves operate on the order of centimeters, rather than nanometers for light sources and have been used for medical imaging for several decades [31-35]. To compensate for the loss in resolution, TAT utilizes an indirect measurement of tissue properties through thermoacoustic waves. Acoustic waves usually travel approximately 1.5 mm/μs in soft tissue and, at megahertz frequencies, can provide excellent spatial resolution of 1mm or better [36].

Upon irradiation by a microwave source, biological samples undergo thermoelastic expansion. In this process, the sample quickly expands and contracts due to energy absorption and dissipation. This process creates an acoustic wave which can be measured with an ultrasonic transducer.

In implementation of this principle, the sample is placed in a mineral oil bath. This bath has relatively low microwave absorbing properties to allow a majority of the microwave energy to reach the sample. However, the acoustic wave easily travels through the media to the transducer.

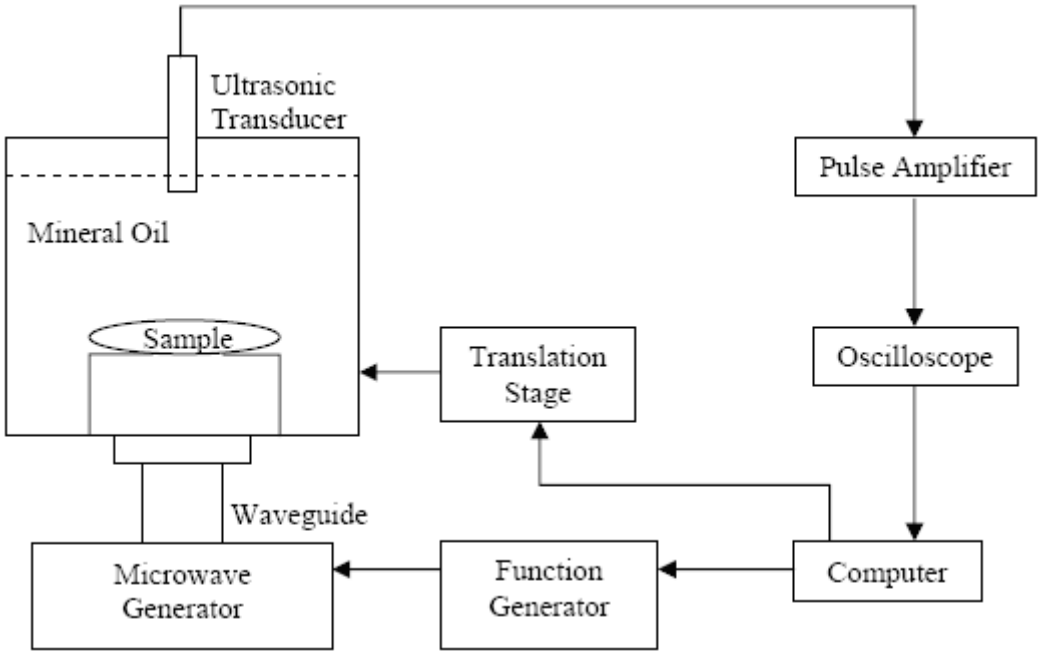

Figure 1. Basic TAT experimental set-up.

Figure 1 shows a forward mode system. Forward mode systems place the irradiation source and ultrasound detection on opposite surfaces of the sample. Conversely, a backward mode system places the irradiation and detection on the same surface of the sample. The microwave pulses are created by a 3GHz microwave generator with a pulse energy of ~5mJ and a pulse width of 0.5μs. The pulses are transmitted to the mineral oil bath by a waveguide with a cross section of 72mm x 34mm.

In this set up, the transducer moves along the y-axis in a linear scan and detects thermoacoustic waves stimulated by a microwave generator. The sample is placed in a mineral oil bath which allows the coupling of the thermoacoustic waves and the ultrasonic transducer.

In nearly every set up, there will be a collection of common components. A computer is used to control the movement of the ultrasonic transducer, as well as store data collected. Also, the computer is connected to a function generator (Protek B-180) which will trigger the microwave source and synchronize the oscilloscope during sampling.

On the receiving side, the signal detected from the transducer (V323, Panametrics), usually in μV, is often very small and must be amplified with a pulse amplifier. The transducer has a central frequency of 2.25MHz and a diameter of 6mm.An oscilloscope (TDS640A, Tektronix) is used for monitoring the experiment and averaging signals. In a typical measurement, the signal detected by the transducer passes through the pulse amplifier. This signal is then recorded and averages 200 times by the oscilloscope and stored on the computer.

After the experiment has completed, the collection of 1D data from the transducer can be combined to create 2D images. However, this method has drawbacks as boundaries in the sample which are parallel to the acoustic axis will not be observed. Thermoacoustic waves usually only travel along the normal of boundaries. As a result only boundaries which are perpendicular, or nearly perpendicular, to the ultrasound transducer will be detected. Still, there are techniques that can increase the image quality with this setup which will be discussed later.

A more sophisticated experimental, set up seen in Figure 2, involves the transducer to rotate around the sample. The reconstruction of data collected is more complicated, but image quality is improved [36].

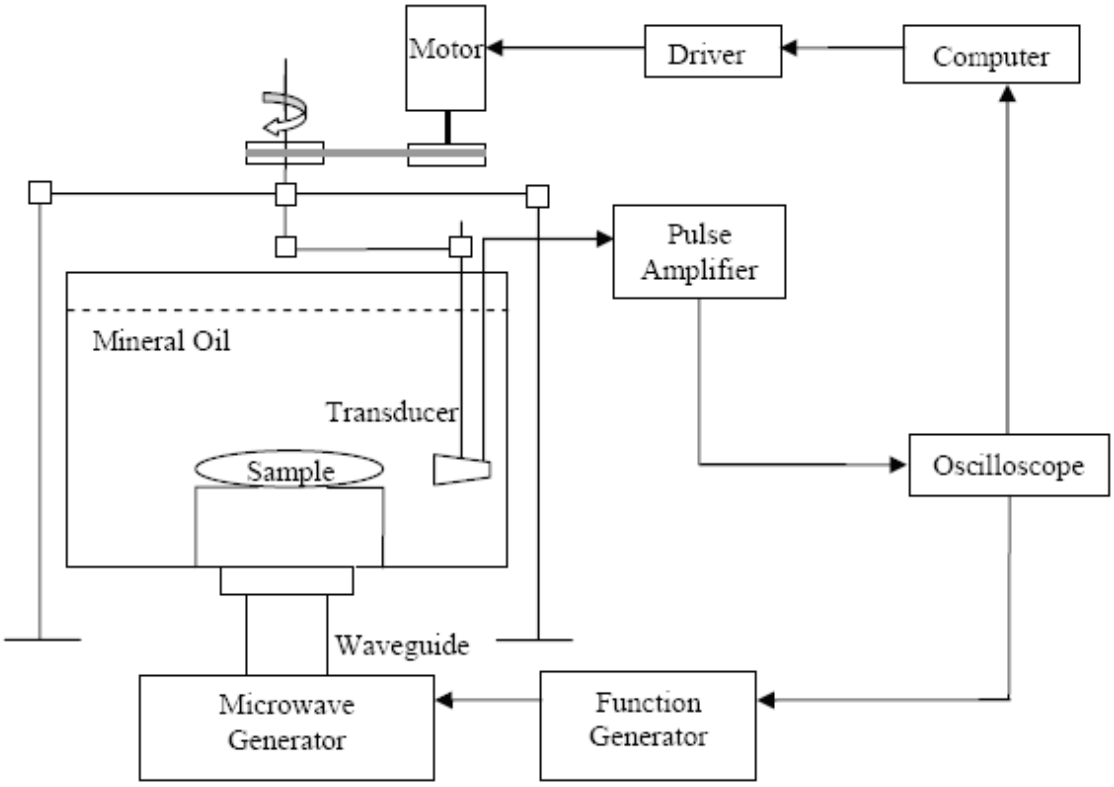

Figure 2. TAT experimental set-up for 2D imaging.

For both set ups, the user has the option of using focused transducers or wideband unfocused transducers. Good images can be acquired from both but require different reconstruction methods.

2.2.1Transduction of Thermoacoustic Waves

The primary mechanism in this technology is the transduction from microwave absorption to heat. The increase in temperature, however, is small, on the order of thousandths of a degree, Kelvin. To simplify the expression of electromagnetic absorption in respect to acoustic waves, the electromagnetic pulse duration is assumed to be much shorter than the thermal diffusion time. This is called the assumption of thermal

confinement [1]. This statement allows the following wave equation to be true, where thermal diffusion can be neglected:

$$\frac{\partial^2 p(r.\bar{t})}{\partial \bar{t}^2} - \Delta^2 p(r,\bar{t}) = \frac{\beta v_s}{C}\frac{\partial H(r,\bar{t})}{\partial \bar{t}} \quad (1)$$

In this expression, $p(r,\bar{t})$ is the acoustic wave related to electromagnetic absorption, $H(r,\bar{t})$; the acoustic speed, v_s, is assumed to be constant; $\bar{t} = tv_s$; C is specific heat; β is the coefficient of volume thermal expansion. This can be rewritten in terms of $H(r,\bar{t})$:

$$p(r,\bar{t}) = \frac{\beta v_s}{4\pi C}\iiint \frac{\partial H(r',t')}{\partial \bar{t}}\frac{dr'}{|r-r'|} \quad (2)$$

$H(r,\bar{t})$ can be further rewritten as the product of a purely temporal component and a purely special component:

$$H(r,\bar{t}) = I_0\phi(r)\eta(\bar{t}) \quad (3)$$

where **Io** scales the incident radiation intensity and $\phi(r)$describes the electromagnetic absorption properties of the sample at **r**. Substitution gives us

$$\phi(r) = \frac{I_0 \beta v_s}{4\pi C} \iiint \phi(r') \frac{d\eta(t')}{\partial t'} \frac{dr'}{|r - r'|} \tag{4}$$

If the absorption properties of the sample and the electromagnetic pulse profile are known, this final expression predicts the pressure outside the tissue. This is useful for theoretical work, but in practice, the inverse problem, in which the absorption properties and profile are unknown, must be solved.

Knowing the propagation velocity of the electromagnetic wave is much greater than the ultrasonic wave, it is safe to assume that the expansion in the sample, due to source pulses, simultaneously causes acoustic waves.

2.2.2 Acquisition and Reconstruction

There are many ways to acquire and reconstruct the data from the ultrasonic transducer [37]. To begin, the type of transducer chosen will determine which reconstruction algorithms are appropriate. A focused transducer is used for linear scans. The reconstruction can be relatively simple by adding the one dimensional data sets together to create two dimensional images. This method is similar to ultrasonography. For the best images, the transducer must have high frequency thermoacoustic wave components. These come from boundaries which are perpendicular to the ultrasonic transducer axis. To further increase the image quality, a large aperture is desirable as the signal to noise ratio is proportional to the square root of the aperture area. However, the resolution will suffer as a result.

Unfocused ultrasonic transducers can be used in multiple set ups. For the reconstruction with unfocused transducers, several options are available. The delay and sum method [38] evenly projects signals to each point within the whole solid angle according to delay. Here, the intensity of every point in the image is the sum of signals from the

transducer at various locations. If the transducer is at *k* different positions, the SNR increases by the square root of *k*.

Another reconstruction method is the modified back projection [39]. This is the inverse solution to the inverse problem mentioned in the previous section. Although exact solutions for the spherical, planar, and cylindrical cases exist, they are computationally intensive and approximations are preferred.

Since the detector is distanced farther away from the sample than the wavelength of high frequency thermoacoustic waves, it can be treated as a point. Following this condition, the inverse solution is:

$$\phi(r) = C \iint_{S_)} dS_0 \cos(\theta_d) \frac{1}{t} \left. \frac{\partial p(r_0, t)}{\partial t} \right|_{t=\frac{|r_0 - r|}{v_s}} \tag{5}$$

where C is a constant, S_o is the surface of detection, and θ_d is the angle between the normal of $d\,S_o$ and $\mathbf{r}\text{-}\mathbf{r}_\mathbf{o}$. As the transducer is moved away from the sample, the resolution increases but signal strength decreases. If the transducer is moved too close, the signal will be strong but the image will be blurred as the detector can no longer be considered a point.

Noise plays a role in the imaging process and usually comes from two sources: background noise and electromagnetic induction due to microwave pumping. The background noise can usually be removed through averaging samples. To reduce the effects of the microwave pumping, simply subtract the signal that is measured when

there is no sample from the experimental data. Furthermore, a Gaussian filter may help as the low frequency components of the acoustic waves are not necessary, as are some of the high frequency components.

One key characteristic of TAT is its scalability. By adjusting the microwave frequency, the depth and contrast can be manipulated. As the wavelength increases, penetration depth increases and contrast decreases. Also, TAT can penetrate at different depths depending on the sample since depth is inversely proportional to the absorption coefficient of the sample. For example, a 3GHz wave can penetrate 9cm into fat and 1.2cm into muscle but a 300MHz source can penetrate 30cm into fat and 4cm into muscle [40].

2.2.3 Contrast in Thermoacoustic Tomography Imaging

Water is the primary absorber of microwave energy in biological samples. This water content enables thermoelastic expansion and, consequently, thermoacoustic waves. However, using water, alone, limits the applicability of this technique. As a result, contrast in TAT may be improved with an exogenous contrast agent. The addition of a contrast agent that absorbs microwave energy more greatly than water allows the identification of features in the sample that may otherwise be unseen. For thermoacoustic tomography, the contrast agent must convert microwave energy to heat more effectively than the water in the sample.

2.3 Exogenous Contrast Agents

Contrast agents are used in a variety of imaging modalities. The primary purpose of exogenous contrast agents is to enable labeling or identification of desired items in the sample. This is commonly achieved through photon emission, magnetic properties, or other properties which differ from the sample.

For X-ray and CT imaging, iodine and barium are common [41,42]. The high atomic number of iodine enables identification of iodine when in biological samples. For gastrointestinal imaging, barium is consumed by the patient and is identified by the presence of a bright region in the image.

For PET, contrast agents are a requirement for imaging. Radionucleides, such as gallium 67, mercury 197, and cesium 137, are injected into a subject [43,44]. The contrast agents quickly decay and positrons are emitted. As nearby electrons are struck by the positrons, gamma rays are released in opposing directions. Gamma rays which arrive to the receiver simultaneously, but in opposing directions, are recorded and an image is constructed.

In microscopy, organic dyes such as green fluorescent protein (GFP) [45] and indocyanine green (ICG) [46] are used to label biological samples. Upon irradiation, these fluorophores absorb light and emit light at a longer wavelength. Thus, they provide contrast by energy conversion.

More recently, the development of quantum dots provides a new form of optical contrast [47-52]. Quantum dots are nanoscale crystals with quantum confined electrons and discrete energy levels. Upon absorption of a photon, the quantum dots reach an excited state. During relaxation, photons are emitted. Quantum dots benefit from broad absorption spectra and narrow emission spectra. Consequently, a single sample may have several quantum dots emitting at varying wavelengths, but all excited with a single source. Unlike, organic fluorophores, these inorganic contrast agents are more resistant to photobleaching.

Magnetic resonance imaging relies upon the magnetic dipole moments of atoms within the sample. To enhance the image, magnetic materials are inserted into the tissue. Currently, iron oxide nanoparticles are in use as an MRI contrast agent [19-25]. The

super paramagnetic properties make them ideal for enhanced T2 relaxation time images. The iron oxide nanoparticles are considered a negative contrast agent, meaning they appear as a dark region in the image. For T1 imaging, a positive contrast agent, Gadolinium is used.

Iron oxide nanoparticles are of particular interest for thermoacoustic tomography. The magnetic properties of the nanoparticles can be coupled to the magnetic field that corresponds with the microwave radiation. Through this coupling, SPION samples may convert microwave energy to heat and serve a TAT contrast agent. Recent work [23] with iron oxide nanoparticles in toluene show heating capabilities under continuous-wave microwave irradiation. These super paramagnetic particles are the focus of this research on contrast agents for TAT.

III. IMPLEMENTATION AND RESULTS

3.1. Electron Paramagnetic Resonance and Ferromagnetic Resonance

Iron oxide nanoparticles have magnetic properties that enable coupling to microwave energy. This is accomplished through spin resonances. Unpaired electrons spin under an applied field, creating a magnetic moment. This is similar to nuclear spins used in magnetic resonance imaging. For electron spin spins, the phenomena are called electron paramagnetic resonance or ferromagnetic resonance [8,9]. The terminology is determined by the nature of the material, paramagnetic or ferromagnetic. Once a magnetic field is applied, the unpaired electrons will align parallel or anti-parallel to the field. The difference between the two distinct energy states is within the microwave region. The effective field determines the Lamor frequency at which the magnetic moments precess.

$$\omega_0 = -\gamma \mu_0 H_{eff} \tag{6}$$

where γ is the gyromagnetic ratio and μ_0 is the permeability of free space.

Iron oxide nanoparticles do not possess a permanent magnetization but do have some asymmetries. As the magnetic vector strays from the steady state, a latent effective field is created in the nanoparticles due to the anisotropy. The unpaired electrons precess about this latent field. During the process, microwave energy is absorbed and some energy is released in the form of heat. By manipulating the size, material and shape of the nanoparticles, the effects of EPR and FMR may be tuned. The iron oxide colloids, by coupling to the microwave energy and releasing heat, provide contrast beyond the water content available in biological tissues.

3.2. Synthesis of Fe_3O_4 Nanoparticles

Extensive work has been done in the development of inorganic nanoparticles [53]. For iron oxide nanoparticles the synthesis follows a precipitation method [54]. Briefly, ferrous chloride and ferric chloride are added in water in a 1:2 molar ratio. In our preparation, 0.86g of Iron(II) Chloride and 2.35g of Iron(III) Chloride are added to 40ml of deionized water in a three-neck flask under argon. While stirring and heated at 80°C, 5ml of ammonium hydroxide is added. After 30 minutes, 1g of Citric Acid in 2ml of deionized water is added. The stirring continues for an additional 90 minutes at 95°C. At this point, the sample has excess citric acid. To remove this, the solution undergoes dialysis against water for 72 hours with at 12-14kDa membrane. For analysis, TEM images and XPS data is collected. The samples are then diluted to one half, fifth, and tenth of the original concentration. This is denoted as 2x, 5x, and 10x, respectively. By back-calculating the iron content in the sample, these dilutions roughly correspond to 20mg/ml, 10mg/ml, 4mg/ml, and 2mg/ml Fe_3O_4, respectively. These concentrations are consistent with those found in research and clinical trials [19,20,24,25]. From a single synthesis procedure, depending on concentration, hundreds of milliliters can be obtained.

3.3. Characterization and Imaging

3.3.1 TEM

After synthesis, small aliquots are taken for imaging. TEM images are taken to verify morphology of the iron oxide nanoparticles. For imaging, carbon film coated grids are glow discharged in an electric field. A drop of the colloid is deposited on the grid and allowed to evaporate. The images of the SPION samples show particles averaging 8nm in diameter. This is consistent with previous work [54].

Figure 3. TEM image of iron oxide nanoparticles. Bar is 20nm.

TEM images, such as Figure 3, are useful for analysis of shape and size of the nanoparticles, but do not yield sufficient information regarding the chemical composition of the sample. For chemical composition, XPS is performed. The samples are left to settle overnight and centrifuged the next day to create a pellet. The supernatant is removed and the remaining pellet is dried in a vacuum oven for one hour. For XPS analysis, the pellet is ground into a powder.

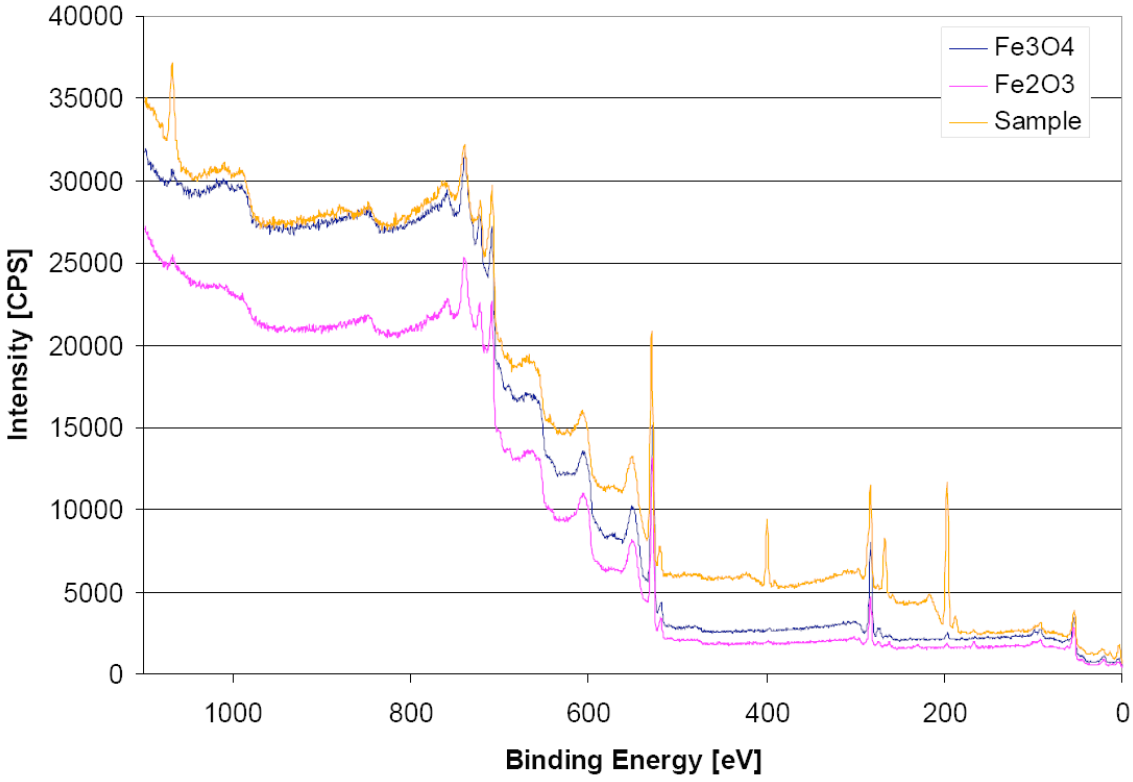

Figure 4. XPS data for commercially available iron oxides and sample.

XPS data are collected for two commercially available iron oxide nanoparticle samples and the Fe_3O_4 sample made in the synthesis described previously. The profiles of the commercial controls and the synthesized sample are compared in Figure 4

The synthesized sample and Fe_3O_4 commercial control have similar profiles. However, there are significant carbon and chloride phases in the synthesized sample. Carbon is a result of the citric acid used to stabilize the nanoparticles, while excess chloride is left over from the synthesis process. The excess of chloride is addressed later.

3.3.2 Coaxial and Capacitor Models

The most important characteristics of the super paramagnetic iron oxide nanoparticles (SPION) for our purpose are the microwave absorption properties. Initially, coaxial and capacitor models are designed for characterization. These models are placed in an Agilent 8510C vector network analyzer (VNA) and the dielectric properties are recorded from 500MHz to 50GHz. The dielectric properties provide insight to resonant frequencies for the SPION samples where microwave absorption is the greatest.

The coaxial model consists of a copper tube with a conducting wire through the center. The nanoparticle solution fills the tube and serves as the dielectric. The dimensions of the model were determined by the coaxial equation:

$$Z = \frac{138}{\varepsilon}\log\left(\frac{D}{d}\right) \tag{7}$$

where D is the inner diameter of the outer conductor, d is the outer diameter of the inner conductor, and ε is the relative dielectric constant. Images of the coaxial and capacitor models are seen in Figure 5.

Figure 5. Coaxial and capacitor models for vector network analyzer measurements.

Assuming the nanoparticle solution is primarily water, the dielectric for this model is approximately 78. From here the design for a 1” diameter copper tube and 22AWG wire provides a coaxial model with an impedance of approximately 25 Ohms. The VNA requires a 50 Ohm device under test (DUT). Although the coaxial model is not impedance-matched, the information of interested needs to only be relative.

The capacitor model is simple in design. Two 1” copper plates are separated with a rubber o-ring. The nanoparticle solution is injected inside the capacitor cavity and the model is connected to the VNA.

In both cases, the models prove unreliable and the data is difficult to interpret. A simpler approach is to simply place the nanoparticle solution in a conventional microwave oven and record the temperature over time [7].

3.3.3 Conventional Microwave Oven

Five control samples of water were placed, one at a time, into the microwave oven. The first sample is measured after 15 seconds. The next sample is placed in the oven and measured at 30 seconds. The temperature of the water is measured every 15 seconds up to 75 seconds. The same procedure is done with iron oxide nanoparticle samples.

The conventional microwave oven experiment shows a qualitative view of the absorption potential of iron oxide nanoparticles. Five samples of water and five samples of iron oxide nanoparticles are placed individually into a microwave oven. Conventional microwave ovens generally operate at 2.45GHz, continuous wave. After the temperature of the sample is measured, a new sample is placed in the oven and irradiated for the next time step. The temperature is measured with a thermocouple, so the sample has to be removed from the microwave for a reading. To avoid cooling effects, a new sample replaces the measured sample and the microwave is run for the new time period.

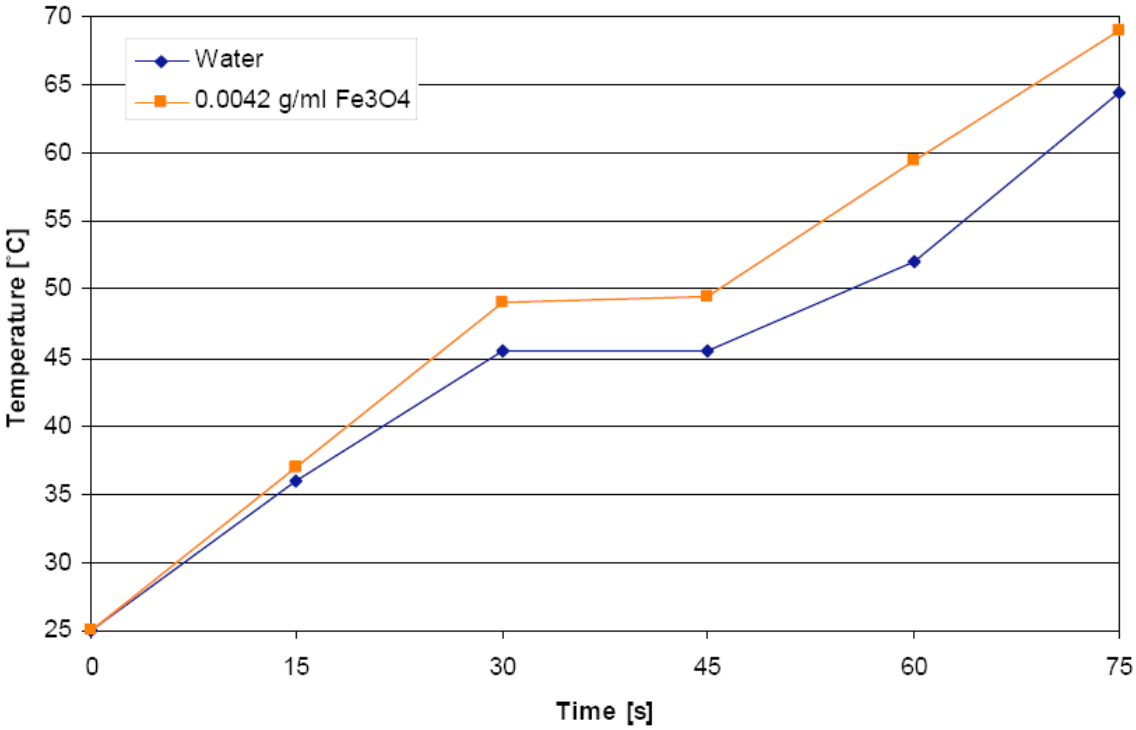

Figure 6. Absorption of water and iron oxide nanoparticles in a microwave oven.

From the plot in Figure 6, water, with the addition of iron oxide colloid, exhibits an improvement of several degrees over water, alone. The microwave oven experiment yields positive qualitative data, but a more thorough characterization is necessary.

3.3.4 Vector Network Analyzer and Dielectric Probe Kit

The microwave oven experiment provides qualitative information, but more detail is needed for the characterization of the nanoparticles. To do this, a vector network analyzer in conjunction with a dielectric probe kit is used [55]. This probe may be inserted into an aqueous SPION solution and measures the dielectric properties of the sample.

SPION samples are diluted to a half, fifth, and tenth of the original concentration. These 40ml samples are placed in the VNA/Dielectric Probe set-up for spectral analysis. The

particles are analyzed from 200MHz to 20GHz. The experiment yields the real and imaginary parts of the dielectric for the sample. This data is then used to calculate the absorption coefficient [4].

$$\alpha = \omega \sqrt{\frac{\mu\varepsilon}{2}\left[\sqrt{1+\left(\frac{\sigma}{\omega\varepsilon}\right)^2}-1\right]} \tag{8}$$

Here, ω is the angular frequency, μ is the permeability, ε is the permittivity and σ is the conductivity.

In the VNA/Probe Kit set-up, the iron oxide nanoparticles are measured at varying concentrations. Initially, the SPION samples had no absorption increase compared to water. However, if the sample is left to settle overnight, a large portion of the particles settle out of the solution. The remaining supernatant has very strong absorbing abilities. The cause of this is yet to be fully understood.

For the remainder of the study, the supernatant of the iron oxide nanoparticle solution is simply referred to as the iron oxide nanoparticle colloid. At each concentration, the iron oxide nanoparticle colloid shows greater absorption than water. This is especially notable in lower frequencies.

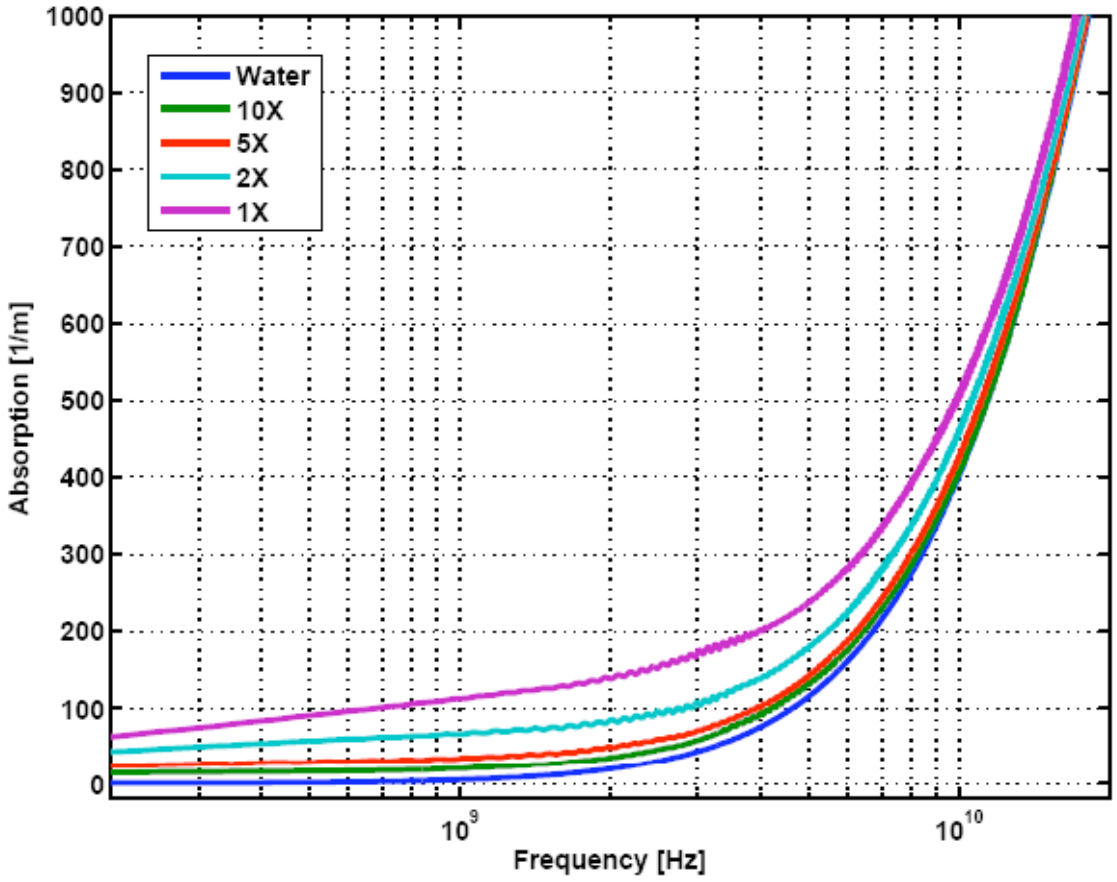

Figure 7. Absorption coefficients of iron oxide nanoparticle colloids in VNA/Probe kit experiment.

Here, in Figure 7, iron oxide nanoparticles are most effective at frequencies below 1GHz, where water absorption is significantly lower when compared to the SPION samples. By normalizing the absorption data relative to water, the advantage of iron oxide nanoparticles is apparent in Figure 8.

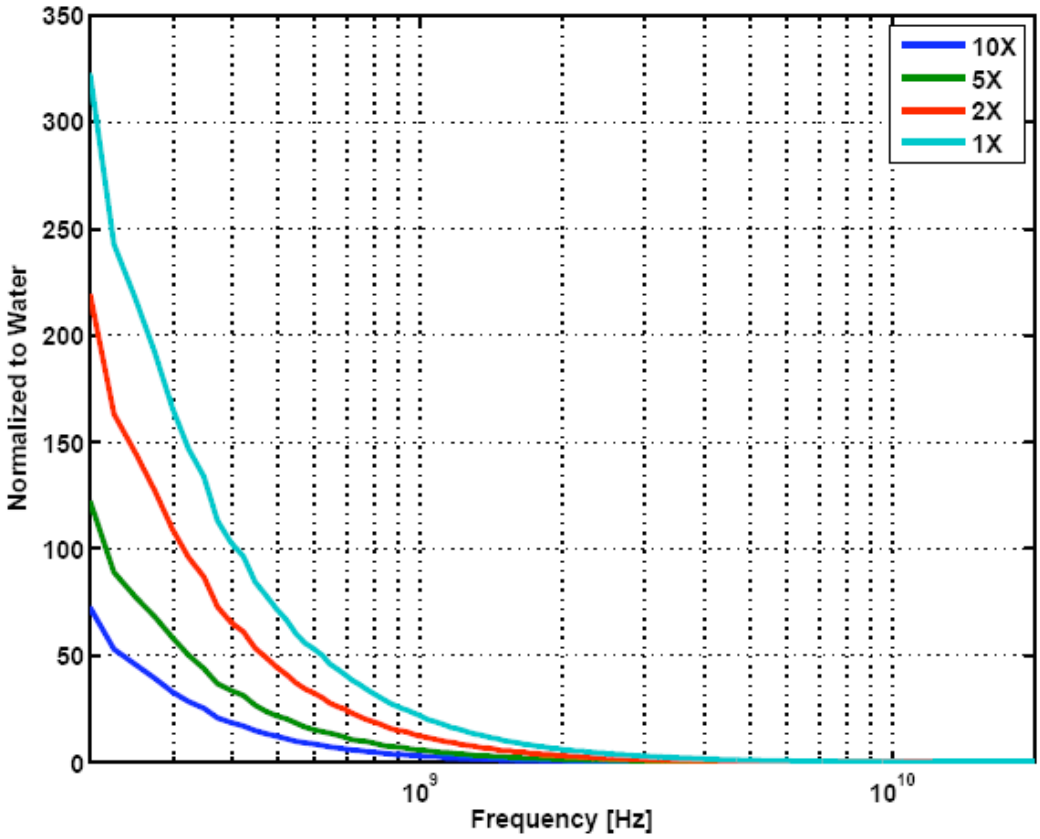

Figure 8. Absorption coefficients of iron oxide nanoparticle colloids normalized to water.

The calculation suggests that at the current operating frequency of the TAT system, 3GHz, there will be some absorption enhancement. However, the iron oxide nanoparticles are significantly more effective in lower frequencies.

3.3.5 One-Dimensional TAT Measurement

Microwave absorption is necessary for the production of a TAT signal. However, the contrast agent must also efficiently undergo thermoelastic expansion. To test this, the SPION samples are placed in the TAT system at a fixed pulsed frequency of 3GHz. This experimental set-up yields a time-resolved acoustic wave of varying amplitude. The strength of the signal corresponds to the absorption properties of the sample under test.

For TAT measurements, the sample is placed in a small tube and immersed in the mineral oil bath. In this experiment, an ultrasonic transducer, fixed in place, records the thermoacoustic waves created by the irradiated sample. This time-resolved data provides relative comparisons in signal strength from the various samples.

In the TAT system, a time-resolved acoustic wave is measured. Each sample is placed in a tube in a mineral oil bath. The TAT system operates at 3GHz. With the transducer fixed in place, one-dimensional thermoacoustic waves are measured. The greater microwave absorption due to nanoparticles is identifiable by the increase in amplitude of the produced acoustic wave. At the highest concentration, 1x, the iron oxide nanoparticle sample has a two-fold increase in thermoacoustic amplitude when compared to water.

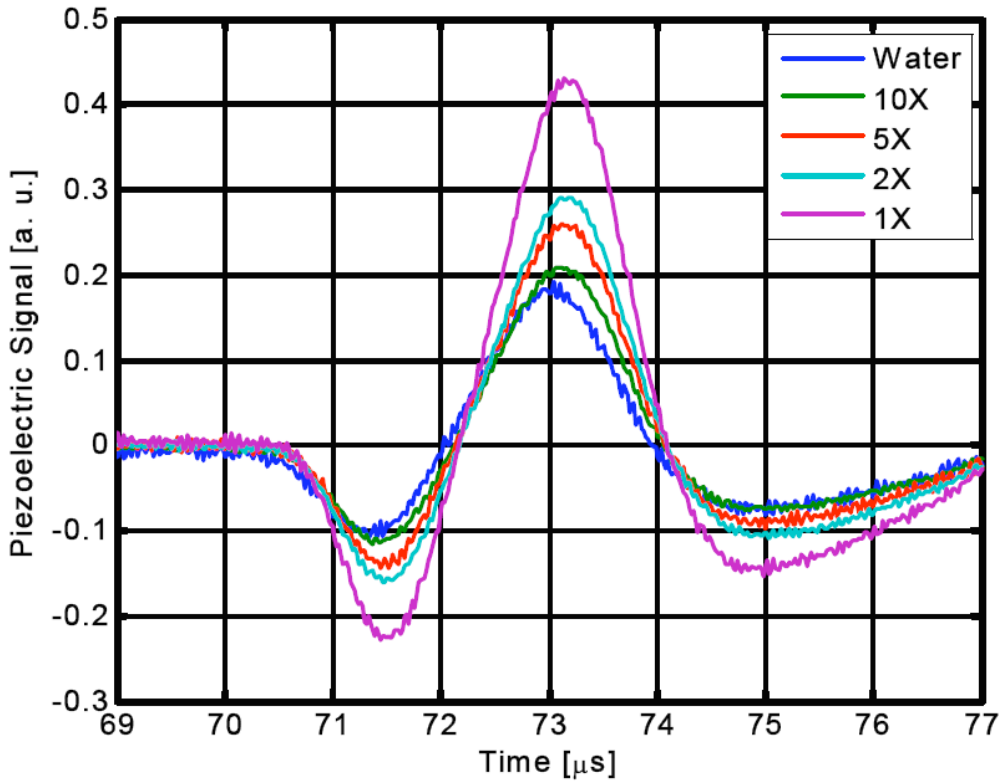

Figure 9. TAT response of iron oxide nanoparticle colloids.

Extracting the data, relative to water, at 3GHz from the VNA experiment from Figure 8 and comparing to the TAT data in Figure 9 shows consistent behavior for the SPION samples. However, the microwave absorption in the VNA experiment is more significant. TAT is an indirect measurement. While the VNA system directly measures dielectric properties, the TAT set-up measures acoustic waves resulting from the microwave properties of the sample. Energy is lost throughout the process of microwave irradiation to thermoacoustic waves. The comparison is available in Figure 10.

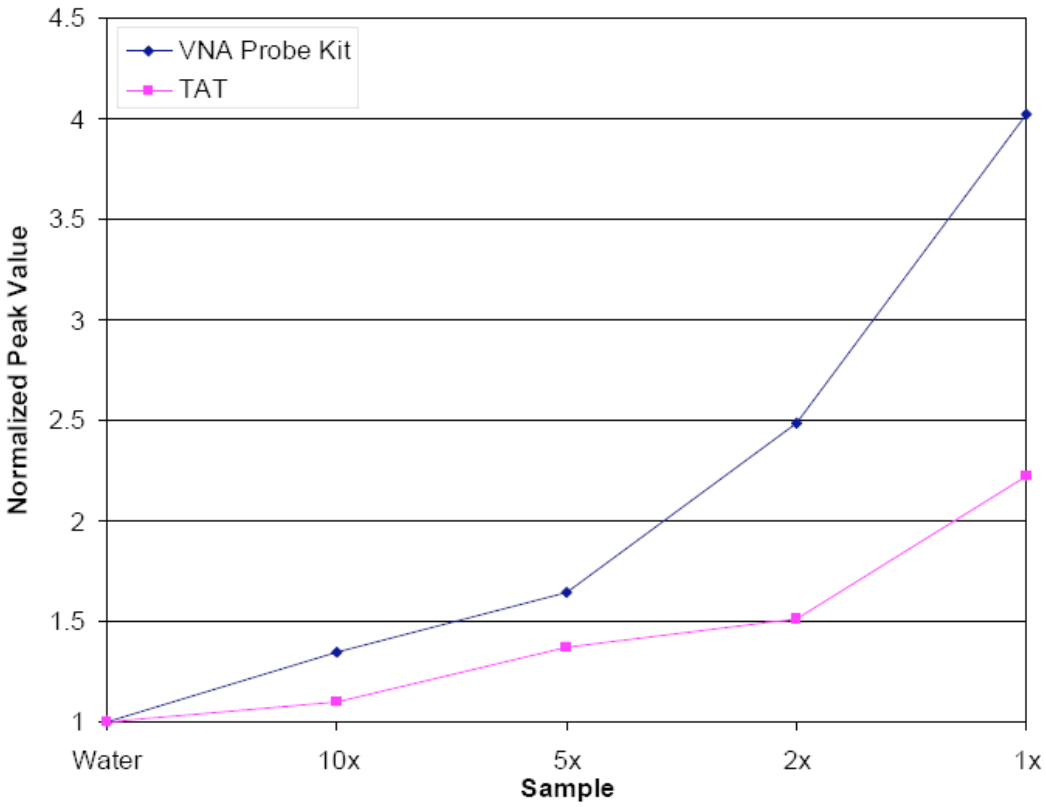

Figure 10. Comparison of relative absorption of iron oxide nanoparticle colloids.

These experiments show the potential benefit of iron oxide nanoparticles as a contrast agent for thermoacoustic tomography. At the highest concentration, microwave absorption is increased by a factor of two at 3GHz for TAT measurements.

3.3.6 Two-Dimensional TAT Imaging

To observe the imaging benefits of a SPION contrast agent, a two dimensional phantom image was taken by inserting four small tubes within porcine fat. Two tubes contained water while the other two tubes were filled with nanoparticle colloid, each with a volume of approximately 0.12ml. As the sample is irradiated by the microwave source, the transducer rotates around the sample and takes measurements. The collection of one-dimensional data is reconstructed into a two-dimensional image in Figure 11.

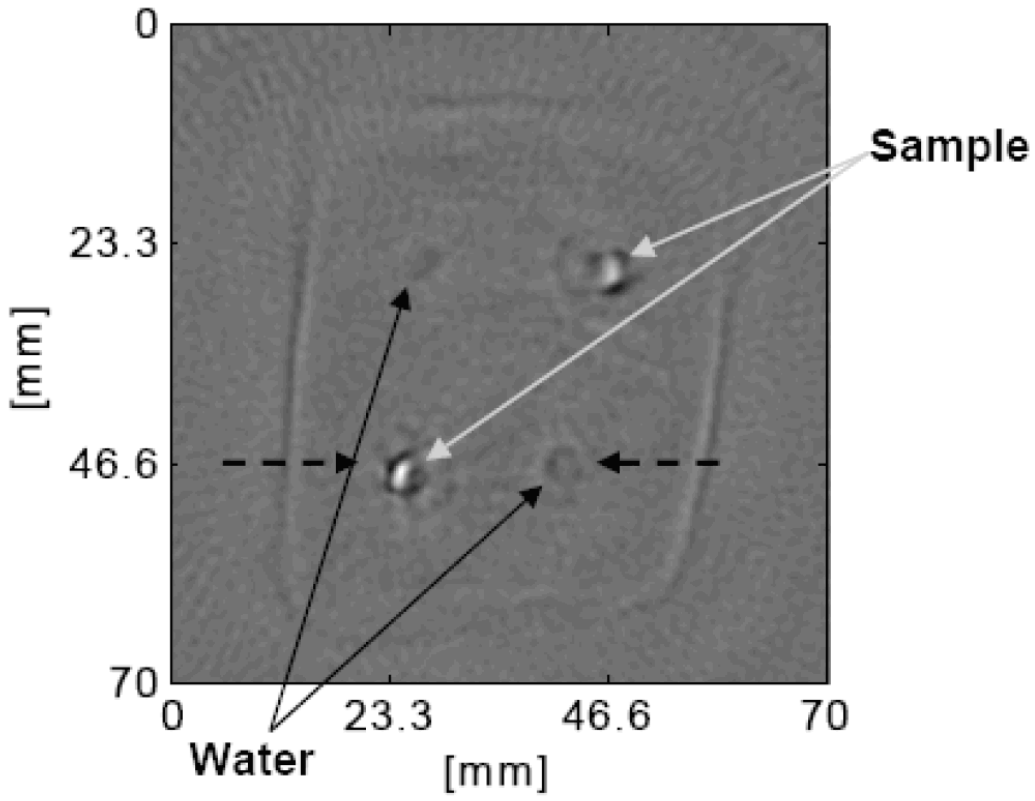

Figure 11. 2D TAT image of phantom model with iron oxide nanoparticle colloid.

In the 2D TAT image, the borders of the porcine tissue and tubes of water and iron oxide colloid are easily identified. Most importantly, the tubes with water are not well defined compared to the iron oxide samples. The noticeable difference in water and iron oxide colloid signify a greater generation of heat by the nanoparticles. In Figure 11, the dotted arrows signify the axis of a one-dimensional reading. The one-dimensional reading, shown in Figure 12, allows a quantitative view on the increase in acoustic wave amplitude.

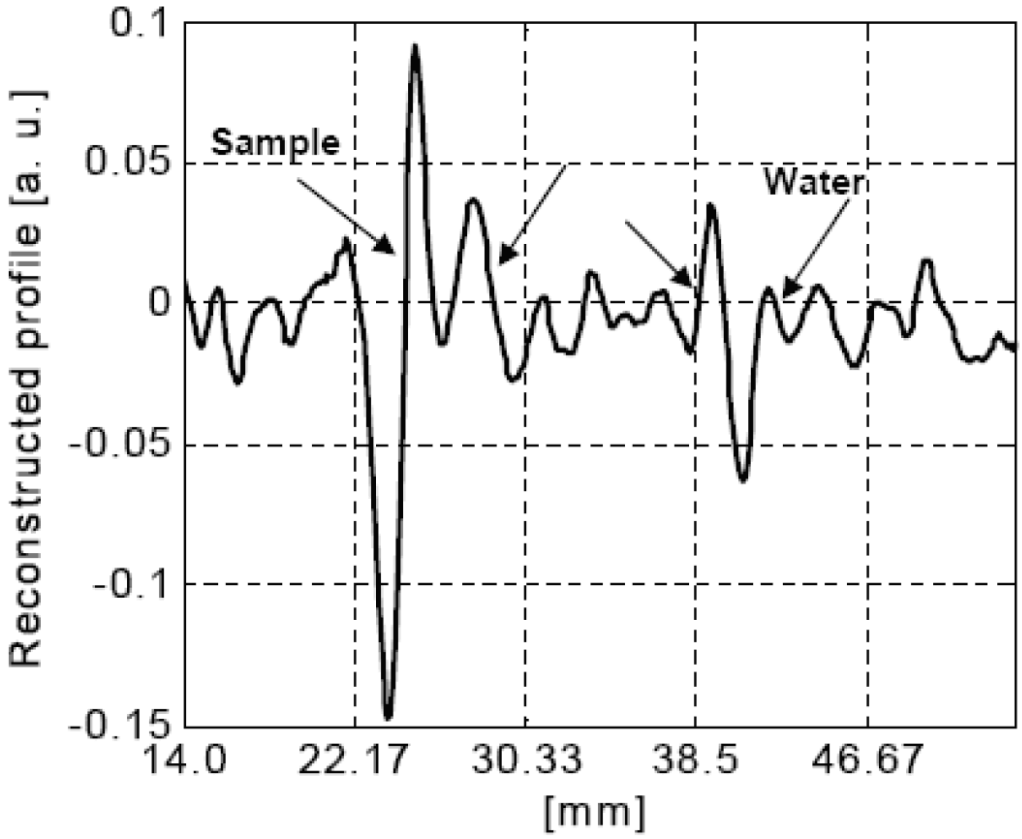

Figure 12. 1D data from 2D phantom model. Data observed along dotted arrows in Figure 11.

Here, the boundaries of the sample and water are easily identified. The iron oxide nanoparticle boundary has a peak-to-peak amplitude nearly twice as large as that of water. This contrast enhancement is visible in the two-dimensional image.

3.3.7. Presence of Citric Acid, Chloride, and Carbon in SPION Sample

All polar molecules can align with an incident electric field. Consequently, other molecules in the SPION samples may have an effect on microwave absorption. For this reason, ferrous chloride, ferric chloride, and citric acid must be examined for microwave absorption. The citric acid used for stabilization is analyzed in the VNA/Dielectric probe kit at 0.1 wt%, 1.0 wt%, and 10.0 wt%. The comparative improvement over water is calculated and plotted in Figure 13. From this data, there is no noticeable microwave absorbing properties for citric acid over the operating frequency range of the TAT system.

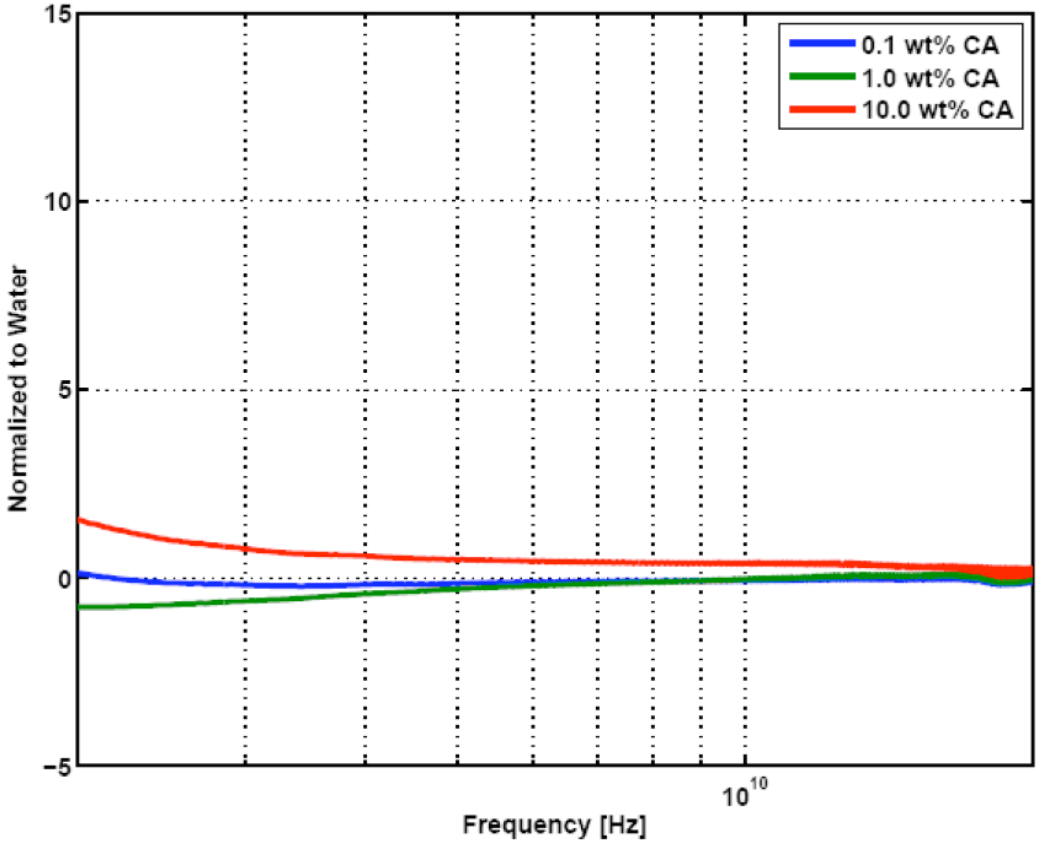

Figure 13. Citric acid absorption in VNA/Probe kit experiment.

From the previous XPS results, there is chloride in the nanoparticle solution. Solutions of ferric and ferrous chloride are made at the concentrations in which they are used in the iron oxide synthesis. These solutions are placed in the TAT system and one-dimensional measurements are made to yield Figure 14.

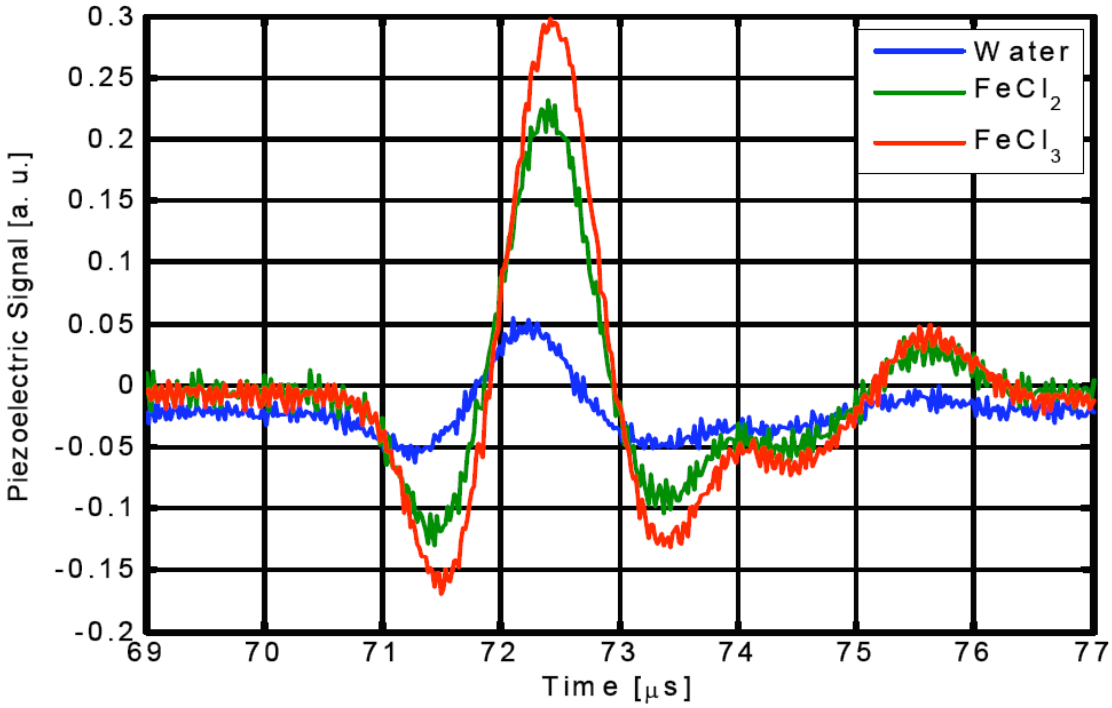

Figure 14. Ferric chloride and ferrous chloride response in 1D TAT measurement.

The results provide a strong argument for the absorbing capabilities of ferric chloride and ferrous chloride. TAT data suggests a 400% to 600% increase in microwave absorption for ferric and ferrous chloride. To avoid observing the effects of these phases, dialysis is performed to remove the excess chloride. After synthesis, the iron oxide colloid is allowed to settle overnight. The next day, the supernatant is removed and placed in a dialysis membrane. After dialysis for 96 hours, the iron oxide samples show no notable absorption.

It is believed the dialysis process has damaged the particles and oxidation has taken effect. As the dialysis time is increased, citric acid is more likely to be removed from the iron oxide nanoparticle solution. Without the citric acid, the particles will aggregate and their magnetic properties will change. Additionally, oxidation takes place over the extended exposure time. The Fe_3O_4 nanoparticles oxidize to Fe_2O_3.

To avoid excessive oxidation, a SPION sample underwent dialysis for 24 hours. EDS data is taken for a sample before and after dialysis. Before dialysis, Figure 15 reveals a significant chloride phase.

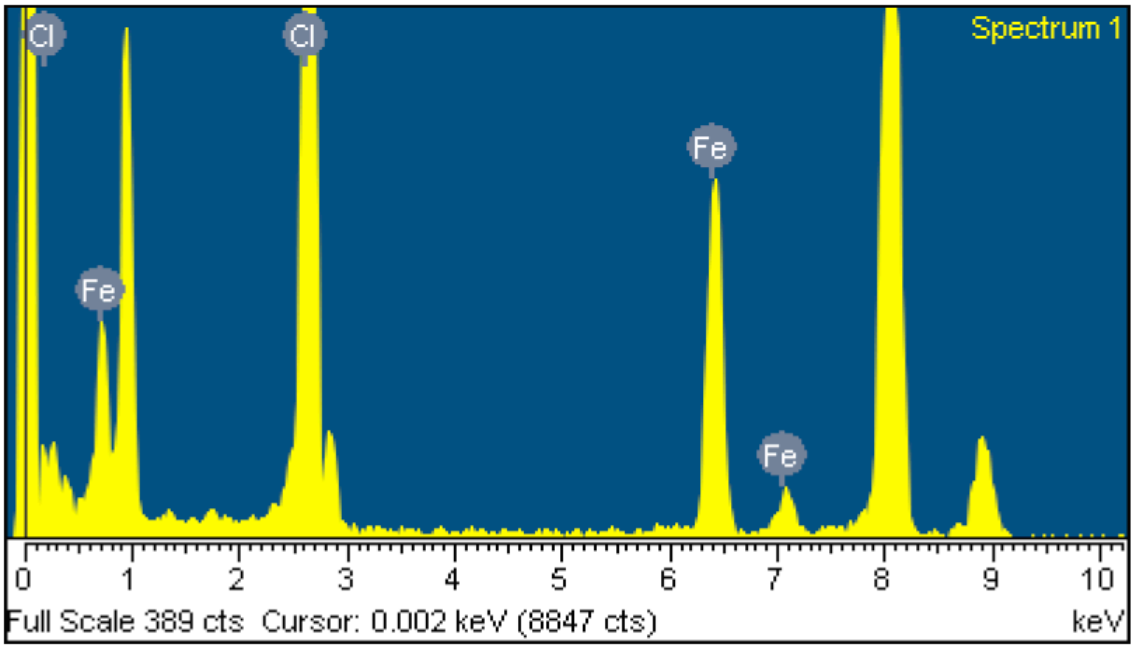

Figure 15. EDS results of SPION sample without dialysis.

After the 24 hour dialysis, the majority of the chloride is removed.

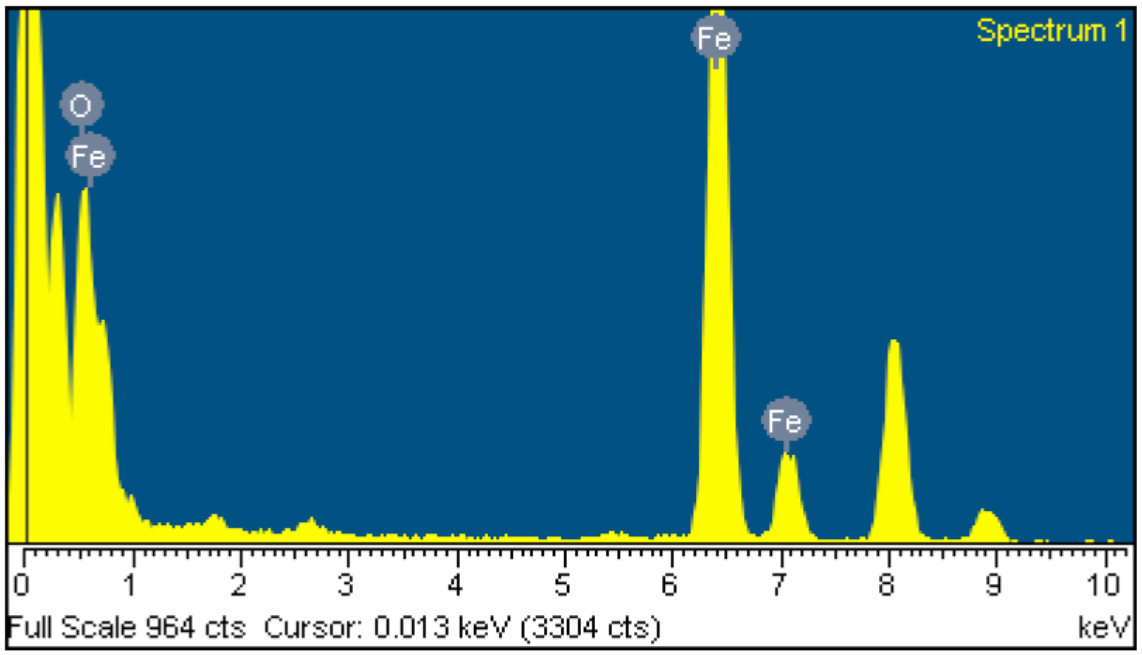

Figure 16. EDS results of SPION sample after 24hr dialysis.

With the majority of the chloride removed in Figure 16, the microwave properties of the particles must be reexamined. The dialyzed sample is placed into the one-dimensional TAT set-up. This sample, with less chloride, still maintains the previously observed behavior of a nearly two-fold increase in thermoacoustic wave amplitude. This result, seen in Figure 17, suggests the iron oxide nanoparticles are the agent causing the conversion of microwave energy to heat.

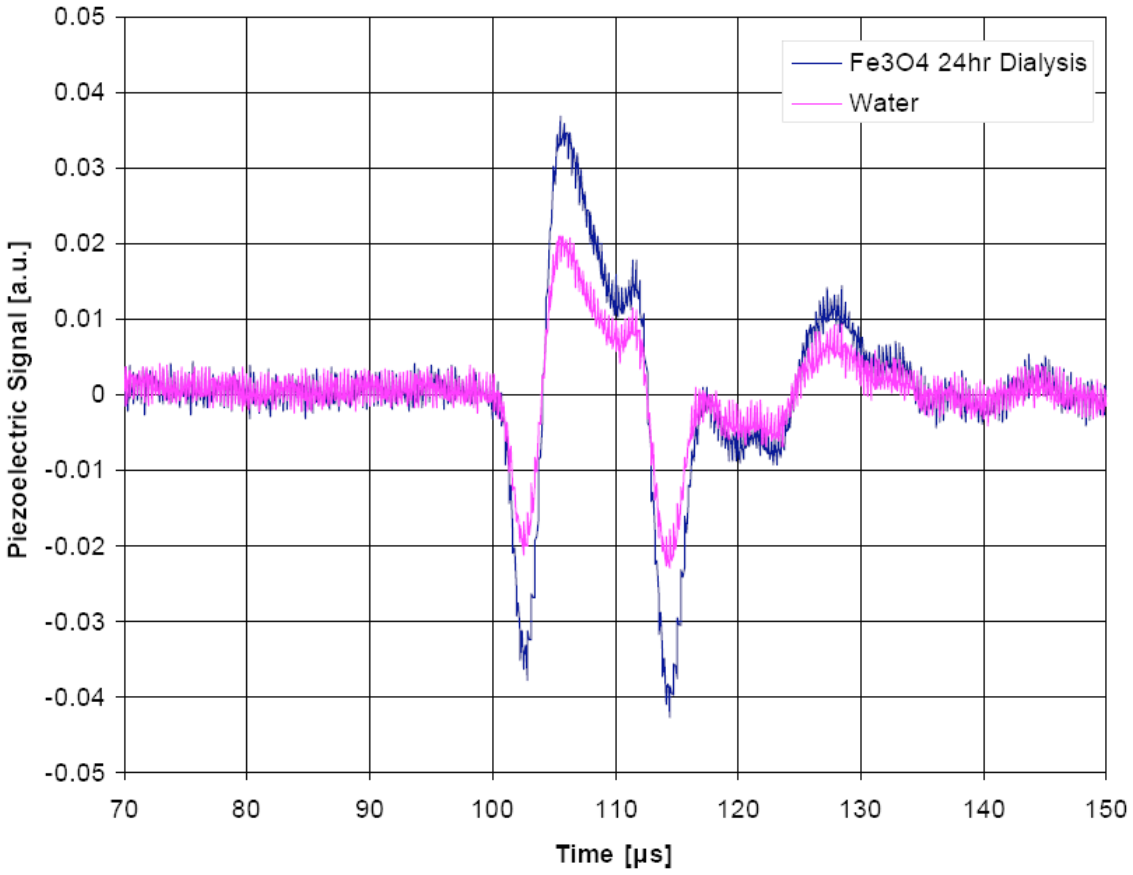

Figure 17. 1D TAT response of water and iron oxide nanoparticle colloid (24hr dialysis).

IV. SUMMARY AND CONCLUSIONS

Thermoacoustic tomography is a powerful hybrid imaging technology. The penetration depth of the microwave source and the resolution of acoustic waves allow early detection of cancerous lesions. Water in the sample absorbs microwave energy to create thermoacoustic waves. Although water content enables TAT imaging, its presence also poses a problem. The strong microwave absorption of water makes it difficult to acquire images with desirable contrast. To overcome this obstacle, an exogenous contrast agent is employed.

Iron oxide nanoparticles are super paramagnetic in nature, and through ferromagnetic resonance, absorb microwave energy. By coupling to the corresponding magnetic field of a microwave source, SPION samples enhance the transduction of microwave energy to heat. This increase in heat creates a thermoacoustic wave up to twice the amplitude of water, alone, as shown in TAT experiments.

Measuring microwave properties of aqueous solutions was found to be most easily accomplished with a vector network analyzer and dielectric probe kit. The system is sensitive to slight movement of the equipment, but after careful calibration, is relatively reliable. The data from this set up is compared to thermoacoustic data at a fixed frequency of 3GHz.

From VNA/Dielectric probe kit data, the largest benefit of iron oxide nanoparticles is observed in lower frequencies. The current TAT system operates at 3GHz. A system operating at 1GHz, or lower, will improve the penetration depth and enable the contrast agent to absorb up to 10 times more effectively than water. This benefit is observed in the relative absorption coefficient data in figure 8.

The synthesis technique still needs refinement. Although encouraging results have been obtained, the ferric and ferrous chloride phases remain in the iron oxide colloid after synthesis and add uncertainty to the results. The large absorption of the two components needs to be fully removed to eliminate their effect on TAT measurements. However, dialysis has proven to be an effected way to remove the majority of the chloride present in the samples.

Currently, the iron oxide nanoparticles are coated in citric acid. This coating enables solubility in water and deters aggregation. Yet, for a more versatile nanoparticle, this coating should be replaced with a more easily adapted surfactant, such as dextran. By changing the outside of the particle, it may now be functionalized for a variety of purposes [56,57].

In addition to the coating, the morphology of the particle must be explored. Although the nanoparticles most closely resemble spheres, they are not perfectly symmetric. This anisotropy can be further exploited by creating nanorods [58-60]. The large aspect ratio will exaggerate the ferromagnetic resonance affect.

Still a nascent field, thermoacoustic tomography contrast enhancement addresses the water absorption challenge. With further development, images with desirable penetration depth, resolution and contrast are attainable. Beyond imaging, thermoacoustic tomography, with iron oxide nanoparticles, may serve as a therapeutic device [61-63]. In this scenario, functionalized nanoparticles will attach to cancerous tumors. Upon irradiation, TAT images will identify the location lesions. With an adjustment in power of the microwave source, the nanoparticles will continue to heat and will thermally ablate the cancer.

REFERENCES

[1] Wang L H 2004 *Journal of Disease Markers* **19** 123

[2] Wang L H, Zhao X, Sun H, and Ku G 1999 *Rev. Scientific Instruments* **70** 3744

[3] Kruger R A, Reinecke D R, and Kruger G A 1999 *Med. Phys.* **26** 1832

[4] Kruger R A, Kopecky K K, Aisen A M, Reinecke D R, Kruger G A, and Kiser, Jr. W L 1999 *Radiology.* **211** 275

[5] Ku G and Wang L H 2000 *Med. Phys.* **27** 1195

[6] Ku G and Wang L H 2001 *Med. Phys.* **28** 4

[7] Kim D, Shahrooz Amin M, Elborai S, Lee S H, Koseoglu Y, Zahn M, and Muhammed M 2005 *J. Applied Phys.* **97** 10J510

[8] Kittel C 1948 *Phys. Rev.* **73** 155

[9] Waldron R A 1959 *British J. Applied Phys.* **11** 69

[10] Huang D, Swanson E, Lin C, Schuman J, Stinson W, Chang W, Hee M, Flotte T, Gregory K, Puliafito C, and Fujimoto J 1991 *Science* **254** 1178

[11] Schmitt J 1999 *J. Selected Topics in Quantum Electronics* **4** 1205

[12] Matsumoto B 2002 *Cell Biological Applications of Confocal Microscopy* (San Diego: Academic Press.) p 507

[13] Wright S J and Wright D J 2002 *Methods Cell Biol.* **70** 1

[14] Diaspro A 2002 *Confocal and Two-Photon Microscopy: Foundations, Applications, and Advances* (New York: Wiley-Liss) p 567

[15] König K 2000 *J. Microscopy* **200** 83

[16] Fukushima E and Roeder S B W 1981 *Experimental Pulse NMR* (Reading, MA: Addison-Wesley)

[17] Stark D D and Bradley W G 1988 *Magnetic Resonance Imaging* (St. Louis, MO: C.V. Mosby Co.)

[18] DeYoe E, Bandettini P, Neitz J, Miller D, and Winans P 1994 *J. Neuroscience Meth.* **54** 171

[19] Wang Y X, Hussain S, and Krestin G 2001 *Eur. Radiol.* **11** 2319

[20] Taupitz M, Schnorr J, Abramjuk C, Wagner S, Pilgrimm H, Hünigen H, and Hamm B 2000 *J. Magnetic Resonance Imaging* **12** 905

[21] Pankhurst Q A, Connolly J, Jones S K, and Dobson J 2003 *J. Applied Phys. D: Applied Phys.* **36** R167

[22] Moore A, Marecos E, Bogdanov, Jr. A, and Weissleder R 2000 *Radiology* **214** 568

[23] Kim D K, Zhang Y, Kehr J, Klason T, Bjelke B, and Muhammed M 2001 *J. Magnetism and Magnetic Mater.* **225** 256

[24] Harisinghani M, Barentsz J, Hahn P, Deserno W, Tabatabaei S, Hulsbergen van de Kaa C, de la Rosette J, and Weissleder R 2003 *New England J. Med.* **348** 2491

[25] Bulte J, Duncan I, and Frank J 2002 *J. Cerebral Blood Flow & Metabolism* **22** 899

[26] Kremkau F 2002 *Diagnostic Ultrasound: Principles and Instruments* (Philadelphia, PA: W. B. Saunder Co.)

[27] Zagzebski J 1996 *Essentials of Ultrasound Physics* (St. Louis, MO: Mosby)

[28] Donald I, MacVicar J, and Brown T G 1958 *Lancet* **1** 1188

[29] Edler I and Hertz C H 2004 *Clin. Physiol. Funct. Imaging* **24** 118

[30] Ohanyido F O 2005 *Healthquest* **3** 23

[31] Bowen T, Nasoni L, Pifer A E, and Sembrosk G H 1981 *Ultrasonography Symposium Procedings* **2** 823

[32] Olsen R G 1982 *Acoustic Imaging* ed. Powers J P (New York: Plenum) p 53

[33] Olsen R G and Lin J C 1983 *Bioelectromagnetics* **4** 397

[34] Lin J C and Chan K H 1984 *IEEE Trans. Microwave Theory Tech.* **32** 854

[35] Nasoni R L, Evanoff, Jr. A, Halverson P G, and Bowen T 1984 *Ultrasonography Symposium Procedings* **5** 633

[36] Xu M, Ku G, and Wang L H 2001 *Med. Phys.* **28** 1958

[37] Xu M, Xu Y, and Wang L H 2003 *IEEE Trans. Biomed. Eng.* **50** 1086

[38] Feng D, Xu Y, Ku G, and Wang L H 2001 *Med. Phys.* **28** 2427

[39] Xu M and Wang L H 2002 *IEEE Trans. Medical Imaging* **21** 814

[40] Xu M, Xu Y, and Wang L H 2003 *IEEE Trans. Biomed. Eng.* **50** 1086

[41] Brandt W and Helms C 1999 *Fundamentals of Diagnostic Radiology* (Philadelphia, PA: Williams & Wilkins)

[42] Johns H and Cunningham J 1983 *The Physics of Radiology* (Springfield, Il: Thomas Books)

[43] Ollinger J and Fessler J 1997 *IEEE Signal Processing Magazine* January 43

[44] Weber W, Avril N, and Schwaiger M 1999 *Strahlenther und Onkologie* **175** 356

[45] Hicks B 2002 *Green Fluorescent Protein: Applications & Protocols (Methods in Molecular Biology)* (Totowa, NJ: Humana Press)

[46] Coscas G 2006 *Atlas of Indocyanine Green Angiography: Fluorescein Angiography, ICG Angiography and OCT Correlations* (Columbia, MD: Elsevier)

[47] Klimov V I 2003 *Los Alamos Science* **28** 214

[48] Alivisatos P 1996 *Science* **271** 933

[49] Parak W, Pellegrino T, and Plank C 2005 *Nanotechnology* **16** R9

[50] Alivisatos P 2004 *Nature Biotechnology* **22** 47

[51] Gao X, Cui Y, Levenson R, Chung L, and Nie S 2004 *Nature Biotechnology* **22** 969

[52] Michalet X, Pinaud F, Bentolila L, Tsay J, Doose S, Li J, Sundaresan G, Wu A, Gambhir S, and Weiss S 2005 *Science* **307** 538

[53] Cushing B, Kolesnichenko V, and O'Conner C 2004 *Chemical Reviews* **104** 3893

[54] Goodarzi A, Sahoo Y, Swihart M, and Prasad P 2004 *Mat. Res. Soc. Symp. Proc.* **789** N6.6.1

[55] Agilent 85070E Dielectric Probe Kit: http://cp.literature.agilent.com/litweb/pdf/5989-0222EN.pdf

[56] Gupta A and Gupta M 2005 *Biomaterials* **26** 3995

[57] Berry C 2003 J. Phys D: *Appl. Phys.* **36** R198

[58] Lian S, Wang E, Kang Z, Bai Y, Gao L, Jiang M, Hu C, and Xu L 2004 *Solid State Communications* **129** 485

[58] Feng L, Jian L, Mai Z, and Zhu D 2004 *J. Colloid and Interface Science* **278** 372

[59] Kumar R V, Koltypin Y, Xu X N, Yeshurun Y, Gendanken A, and Felner I 2001 *J. Appl. Phys.* **89** 6324

[60] Gonsalves K E, Li H, and Santiago P 2001 *J. Materials Science* **36** 2461

[61] Hergt R, Andra W, d'Ambly C, Hilger I, Kaiser W, Richter U, and Schmidt H 1998 *IEEE Transactions on Magnetics* **34** 3745

[62] Johannsen M, Gneveckow U, Eckelt L, Feussner A, Waldöfner N, Scholz R, Deger S, Wust P, Loening S A, and Jordan A 2005 *International Journal of Hyperthermia* **21** 637

[63] Neuberger T, Schöpf B, Hofmann H, Hofmann M, Von Rechenberg B, Häfeli U, and Zborowski M 2005 *J. Magnetism and Magnetic Materials* **293** 483

VITA

Aaron Lopez Keho received his Bachelor of Science degree in electrical engineering from Rice University in 2004. He joined Texas A&M University in August 2004 and received his Master of Science degree in biomedical engineering in August 2006.

Mr. Keho may be reached at Texas A&M University, Department of Biomedical Engineering, 337 Zachry Engineering Center, 3120 TAMU, College Station, TX 77843.